# ArXiv:Astro-ph, Oct 19-23, 2015

от Сильченко О.К.

# Astro-ph: 1510.04696

## Beyond 31 mag/arcsec$^2$: the low surface brightness frontier with the largest optical telescopes

Ignacio Trujillo[1,2] ⋆ and Jürgen Fliri[1,2]
[1]*Instituto de Astrofísica de Canarias, c/ Vía Láctea s/n, E-38205, La Laguna, Tenerife, Spain*
[2]*Departamento de Astrofísica, Universidad de La Laguna, E-38206, La Laguna, Tenerife, Spain*

**ABSTRACT**

The detection of optical surface brightness structures in the sky with magnitudes fainter than 30 mag/arcsec$^2$ (3$\sigma$ in 10×10 arcsec boxes; r-band) has remained elusive in current photometric deep surveys. Here we show how present-day 10 meter class telescopes can provide broadband imaging 1.5-2 mag deeper than most previous results within a reasonable amount of time (i.e. <10h on source integration). In particular, we illustrate the ability of the 10.4 m Gran Telescopio de Canarias (GTC) telescope to produce imaging with a limiting surface brightness of 31.5 mag/arcsec$^2$ (3$\sigma$ in 10×10 arcsec boxes; r-band) using 8.1 hours on source. We apply this power to explore the stellar halo of the galaxy UGC00180, a galaxy analogous to M31 located at ~150 Mpc, by obtaining a surface brightness radial profile down to $\mu_r$~33 mag/arcsec$^2$. This depth is similar to that obtained using star counts techniques of Local Group galaxies, but is achieved at a distance where this technique is unfeasible. We find that the mass of the stellar halo of this galaxy is ~4×10$^9$M$_\odot$, i.e. 3±1% of the total stellar mass

# Наблюдения

## 2 THE DATA

Ultra deep observations of the galaxy UGC00180 and its surrounded region were carried out at the Gran Telescopio de Canarias (GTC) with the OSIRIS (Optical System for Imaging and low-Intermediate-Resolution Integrated Spectroscopy) camera. OSIRIS total field of view (FOV) is 7.8′×8.5′, of which 7.8′×7.8′are unvignetted. The OSIRIS camera is composed of two CCDs with a gap of 9.4″between them. The pixel scale of the camera is 0.254″. The images were obtained using the Sloan r' filter during 6 (non-consecutive) nights. Images were taken under good seeing conditions, producing a final image with a Full Width Half Maximum (FWHM) seeing of ∼0.9″.

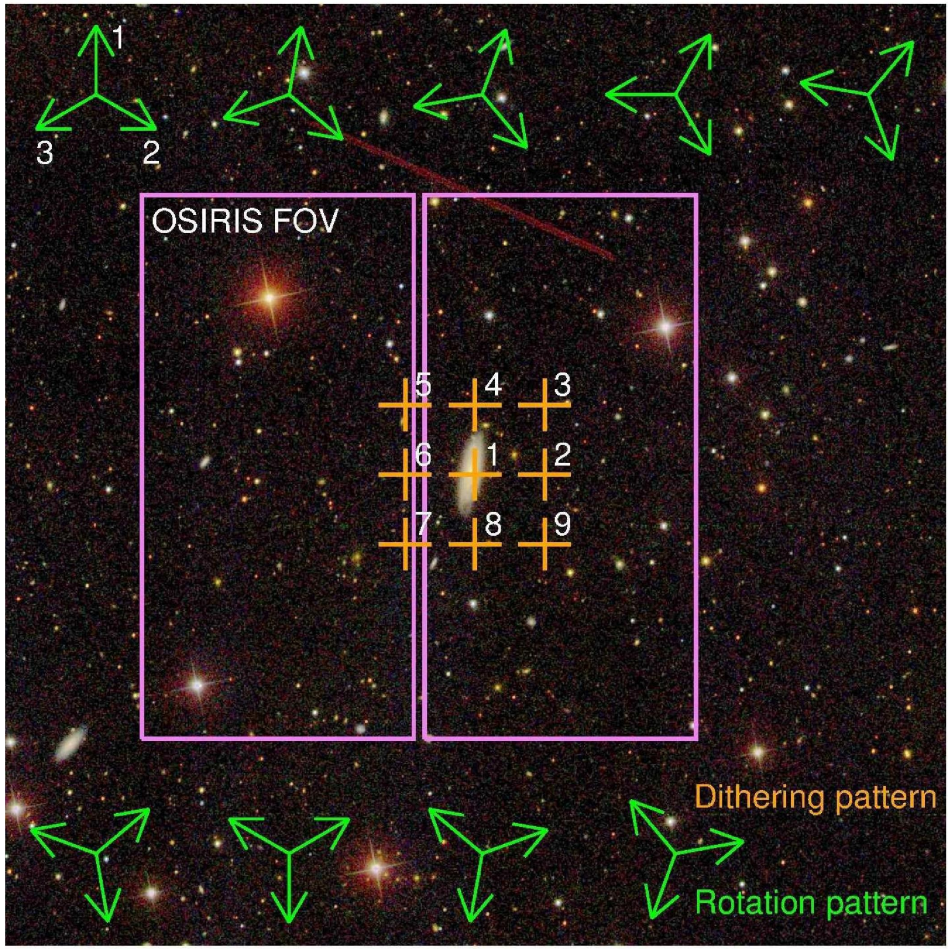


**Figure 1.** Dithering and rotation sequence followed to get the final image. The background image is a color composite of the UGC00180 region obtained from SDSS. The total field of view of the SDSS image corresponds to 13.5′×13.5′. The field of view of each pointing by the OSIRIS camera (7.8′×7.8′) is overplotted with a violet contour. The position of the orange crosses indicate the dithering pattern followed in each block of observations, whereas the green arrow indicates the position angle of the camera in each set of observations. In total, the final image is composed by 3×9×9 pointings. A full description of the procedure is done in the text.

### 2.8 Image coaddition

Once the astrometry of every individual science image is recalculated to a common astrometric solution and the images are calibrated as well as sky subtracted, we use SWarp (Bertin et al. 2002) to put all our data into a common grid. SWarp is a program that resamples and co-adds together FITS images using any arbitrary astrometric projection defined in the WCS standard. The combination uses the median of those images. The common field of view is illustrated in Fig. 2. The image resampling method that was used is LANCZOS3.

The final coadded image (see Fig. 3) is significantly much deeper than the individual exposures and low surface brightness features, hidden in the individual exposures, emerge in the final stacking. These low surface brightness features (extended dust emission, halos of bright stars, etc) affect to the sky determination of our individual science images. For this reason, it is necessary to

# Окончательный суммарный вид

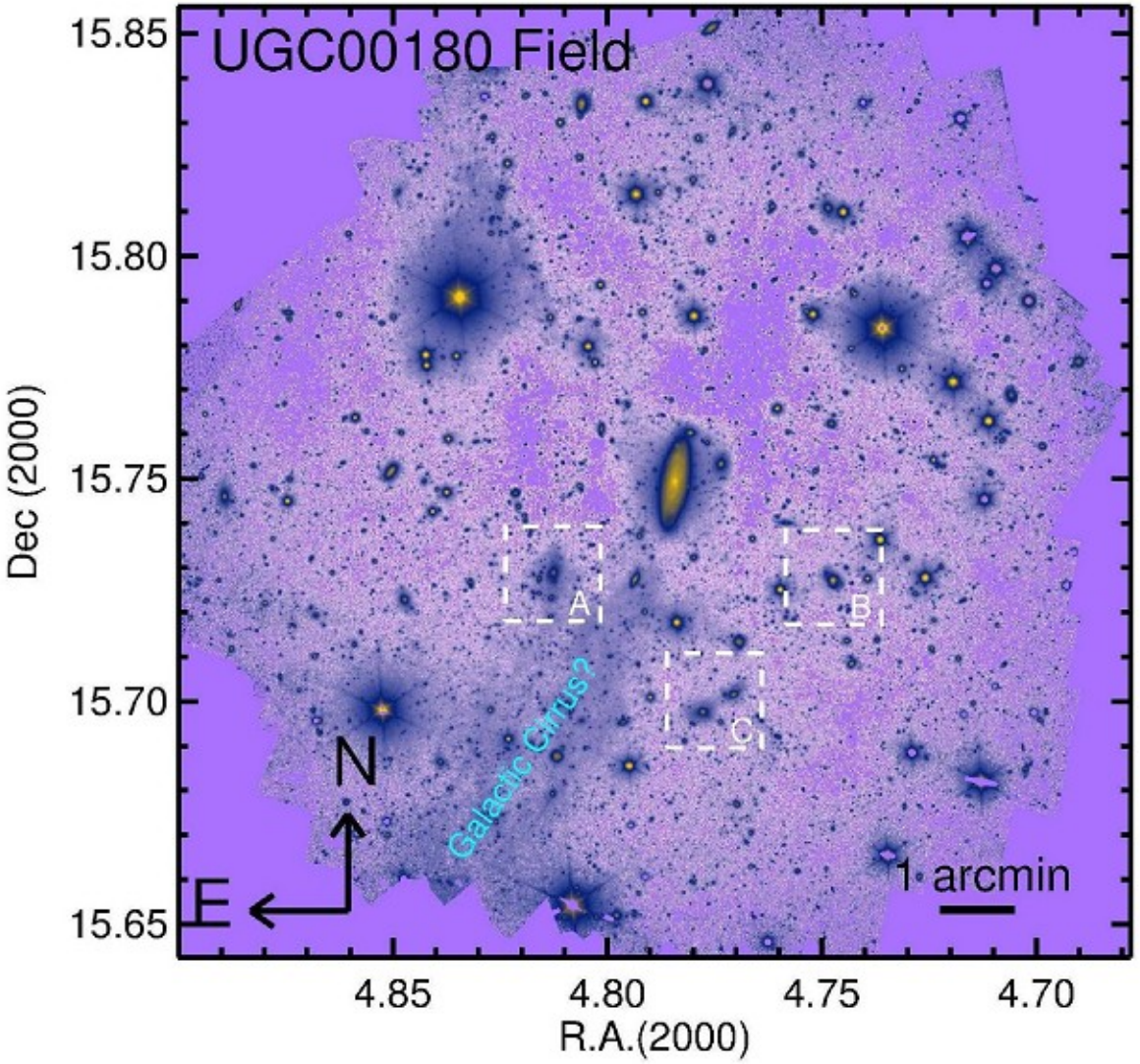

# Фоновые объекты

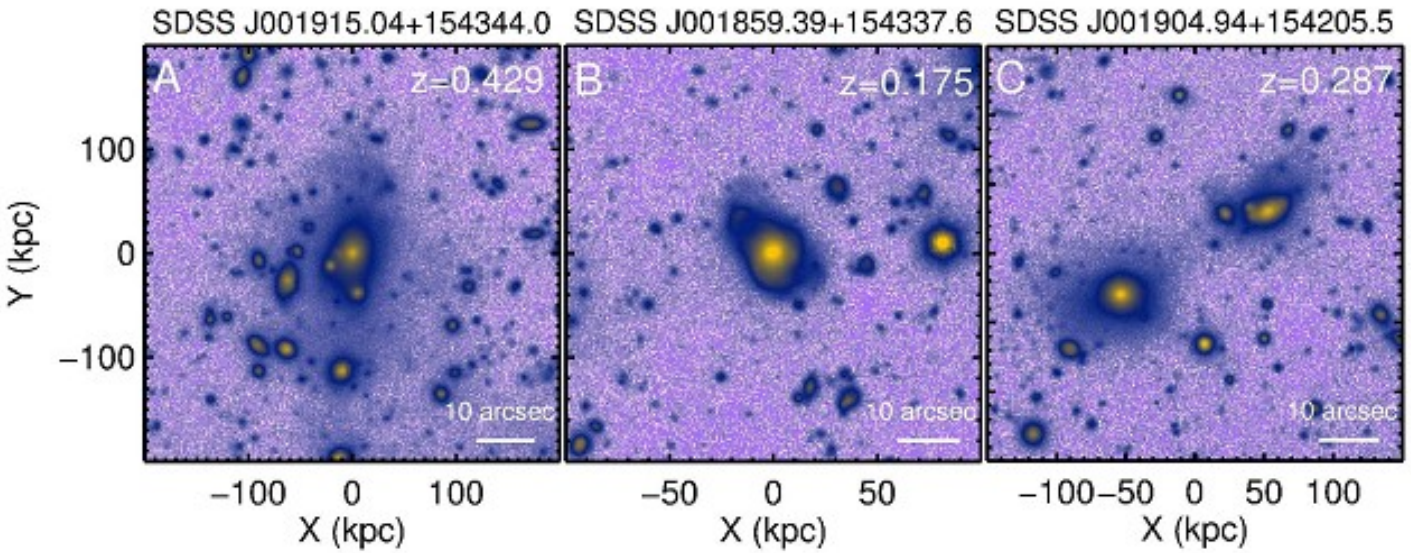


**Figure 5.** Zoom-in to some of the interesting astronomical objects located nearby UGC00180. Panel A shows a cluster of galaxy at z=0.429. The image is deep to enough to show the extended intra cluster light of this object up to distances of 150 kpc. Panel B and C illustrate the merging activity in a galaxy located at z=0.175 and a galaxy pair at z=0.287. The redshifts used are all photometric and obtained from the SDSS catalogue Photoz. More information can be found here https://www.sdss3.org/dr10/algorithms/photo-z.php

# Борьба за PSF

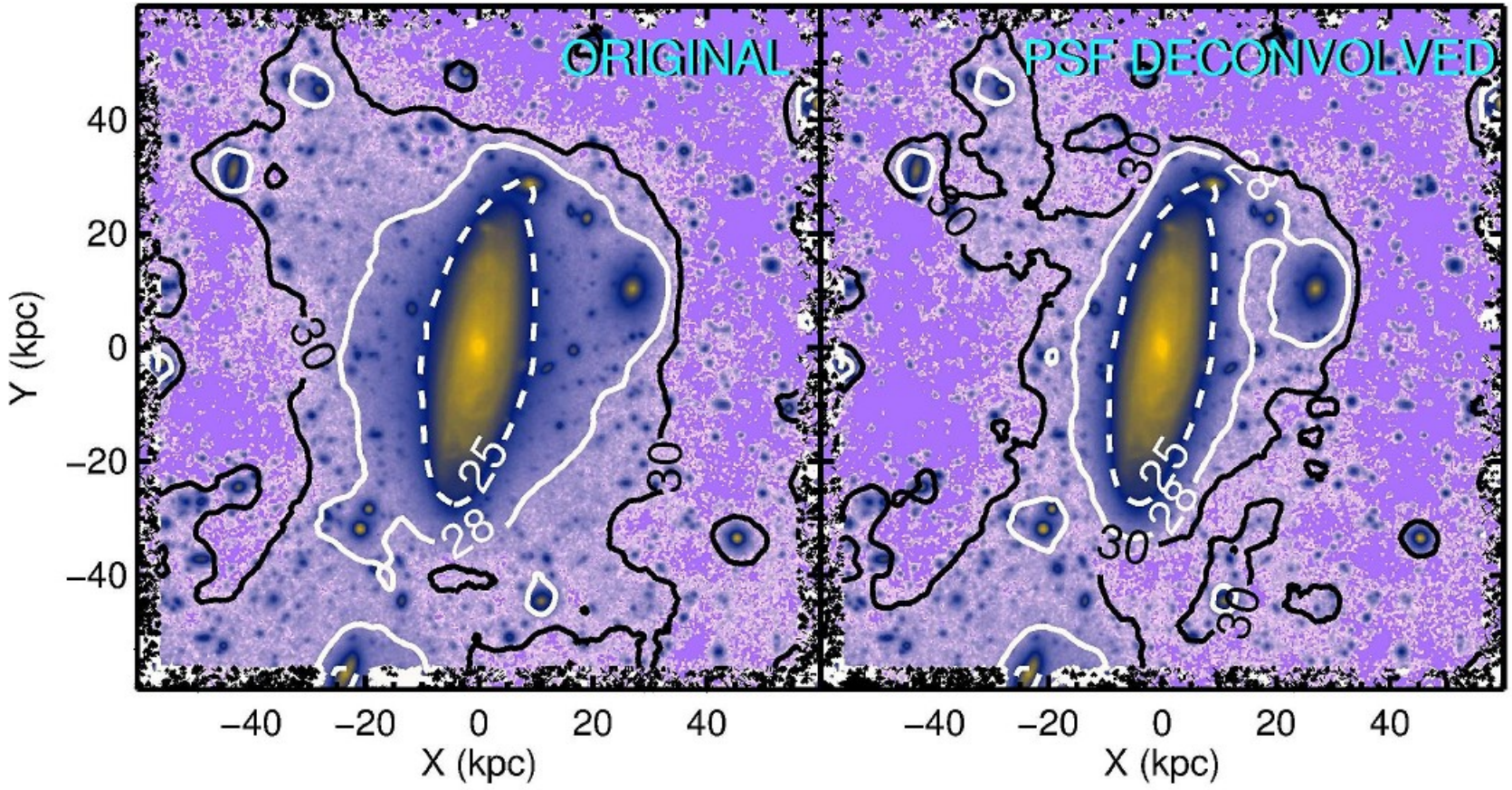


**Figure 10.** The effect of the PSF on the surface brightness distribution of UGC00180. The figure shows the dramatic effect of the PSF on the surface brightness distribution on the isophotal contours of the galaxy. We indicate the position of the 25, 28 and 30 mag/arcsec$^2$ isophotes. The effect of the PSF is particularly relevant when reaching surface brightness fainter than 25 mag/arcsec$^2$ (r-band).

# Окончательный профиль яркости

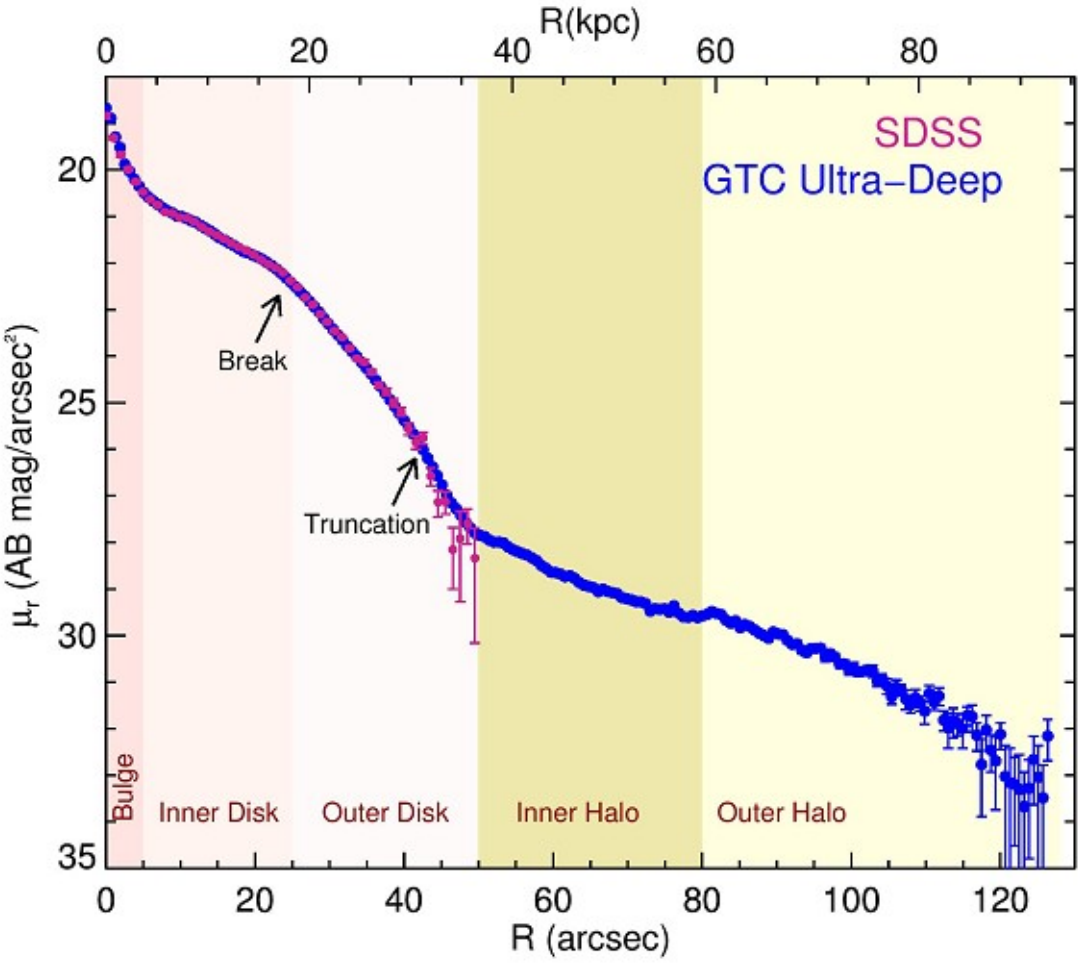

# Astro-ph: 1510. 05009

SPECTROSCOPIC STUDY OF STAR-FORMING GALAXIES IN FILAMENTS AND THE FIELD AT $z \sim 0.5$: EVIDENCE FOR ENVIRONMENTAL DEPENDENCE OF ELECTRON DENSITY

Behnam Darvish,[1] Bahram Mobasher,[1] David Sobral,[2,3,4] Shoubaneh Hemmati,[1] Hooshang Nayyeri,[5] Irene Shivaei [1]

*Accepted for publication in the ApJ*

ABSTRACT

We study the physical properties of a spectroscopic sample of 28 star-forming galaxies in a large filamentary structure in the COSMOS field at $z \sim 0.53$, with spectroscopic data taken with the Keck/DEIMOS spectrograph, and compare them with a control sample of 30 field galaxies. We spectroscopically confirm the presence of a large galaxy filament ($\sim$ 8 Mpc), along which five confirmed X-ray groups exist. We show that within the uncertainties, the ionization parameter, equivalent width (EW), EW versus specific star-formation rate (sSFR) relation, EW versus stellar mass relation, line-of-sight velocity dispersion, dynamical mass, and stellar-to-dynamical mass ratio are similar for filament and field star-forming galaxies. However, we show that on average, filament star-forming galaxies are more metal-enriched ($\sim 0.1-0.15$ dex), possibly due to the inflow of the already enriched intrafilamentary gas into filament galaxies. Moreover, we show that electron densities are significantly lower (a factor of $\sim$17) in filament star-forming systems compared to those in the field, possibly because of a longer star-formation timescale for filament star-forming galaxies. Our results highlight the potential pre-processing role of galaxy filaments and intermediate-density environments on the evolution of galaxies, which has been highly underestimated.

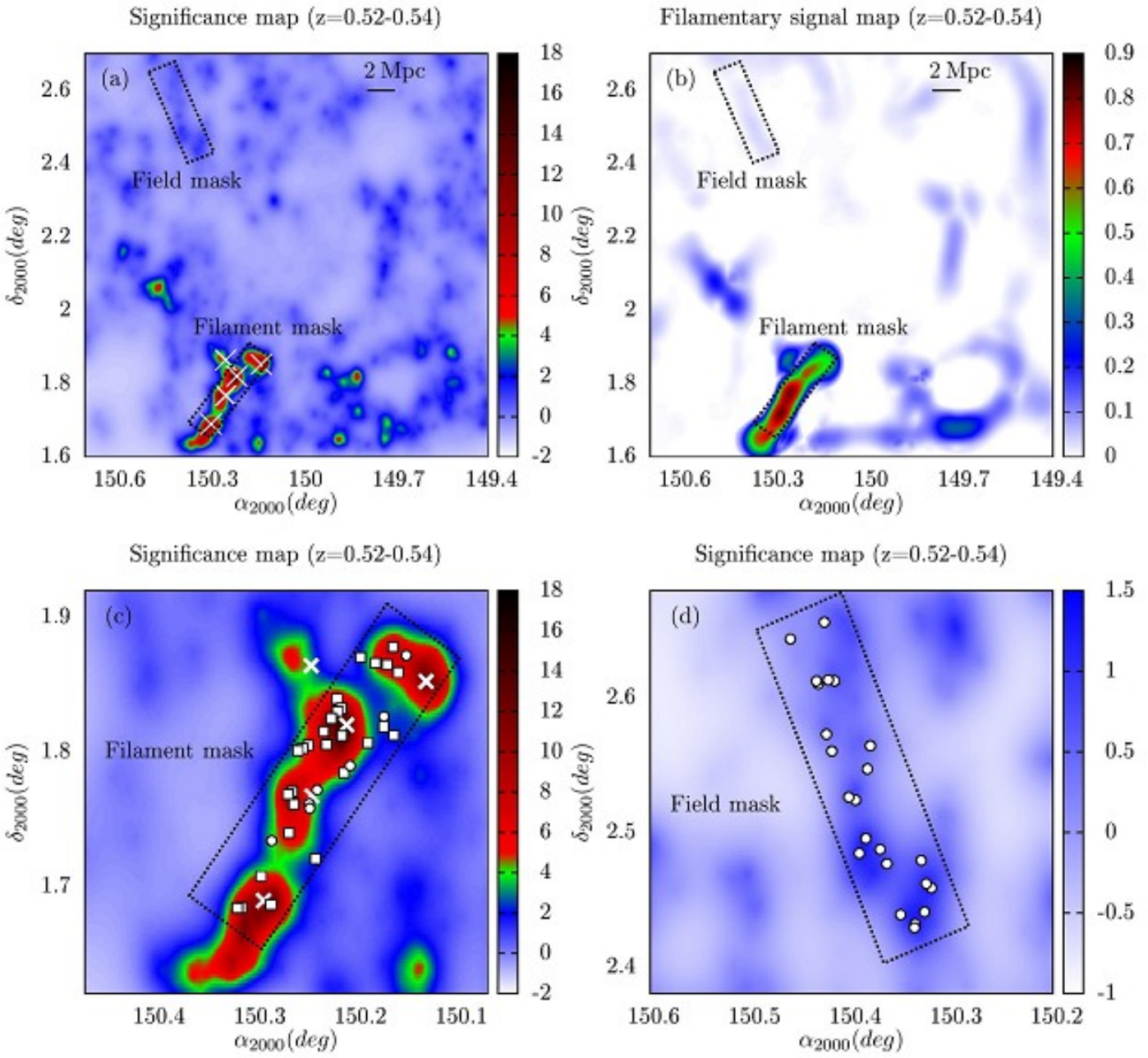
Significance map (z=0.52-0.54)
(a)
2 Mpc
Field mask
Filament mask
$\delta_{2000}(deg)$
$\alpha_{2000}(deg)$
Filamentary signal map (z=0.52-0.54)
(b)
2 Mpc
Field mask
Filament mask
$\delta_{2000}(deg)$
$\alpha_{2000}(deg)$
Significance map (z=0.52-0.54)
(c)
Filament mask
$\delta_{2000}(deg)$
$\alpha_{2000}(deg)$
Significance map (z=0.52-0.54)
(d)
Field mask
$\delta_{2000}(deg)$
$\alpha_{2000}(deg)$

# Спектры с DEIMOS/Keck

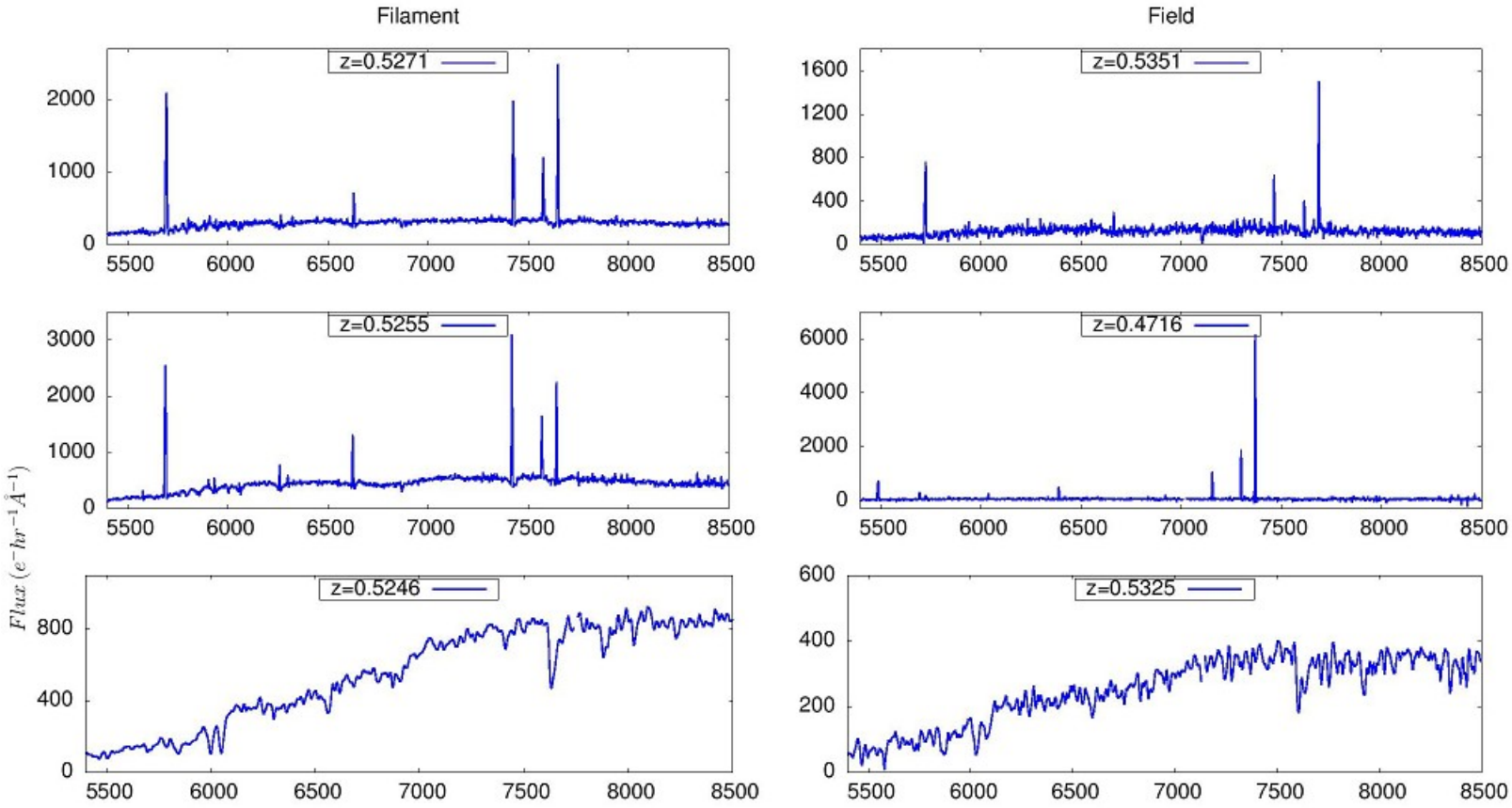

# Много чем они похожи…

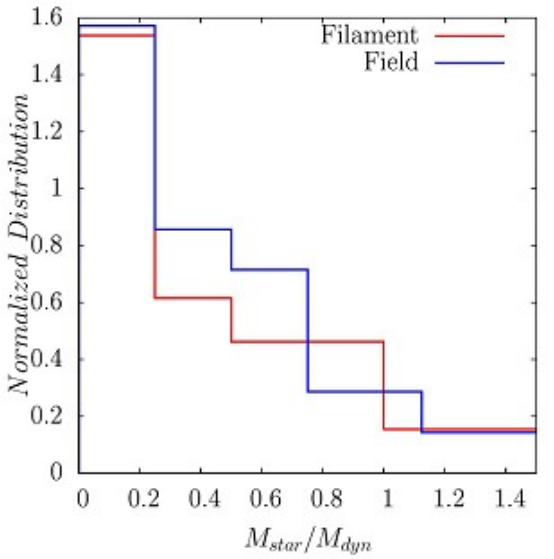


FIG. 15.— Normalized distribution of stellar-to-dynamical mass ratio ($M_{star}/M_{dyn}$) for filament (red points) and the field (blue points) star-forming galaxies. We do not find a significant difference between them. After discarding the unphysical $M_{star}/M_{dyn}$ >1 data from our analysis, we find that for filament star-forming galaxies, the median stellar-to-dynamical mass ratio is $M_{star}/M_{dyn}$ ~0.28 with a median absolute deviation ~0.15, fully consistent with the field star-forming galaxies (median $M_{star}/M_{dyn}$ ~0.27 and median absolute deviation 0.15). The K-S test also shows no significant difference between the distribution of $M_{star}/M_{dyn}$ in filament and the field (p-value=0.47).

- Например, долей барионной массы…
- А также типичным темпом звездообразования, типичной массой галактики, и тд

# А вот чем они не похожи, так это металличностью и эл. плотностью

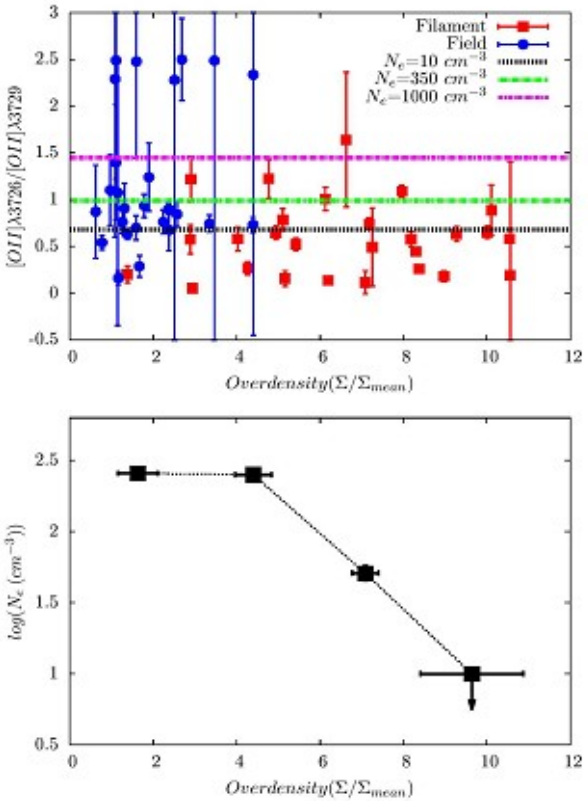


FIG. 8.— Top: [OII]λ3726/λ3729 line ratio for filament (red points) and field (blue points) star-forming galaxies as a function of local overdensity of galaxies. The line ratios that correspond to electron densities of $N_e$=10, 350, and 1000 $cm^{-3}$ are shown with black, green, and pink dashed lines, respectively. We find that filament star-forming galaxies tend to have lower electron density

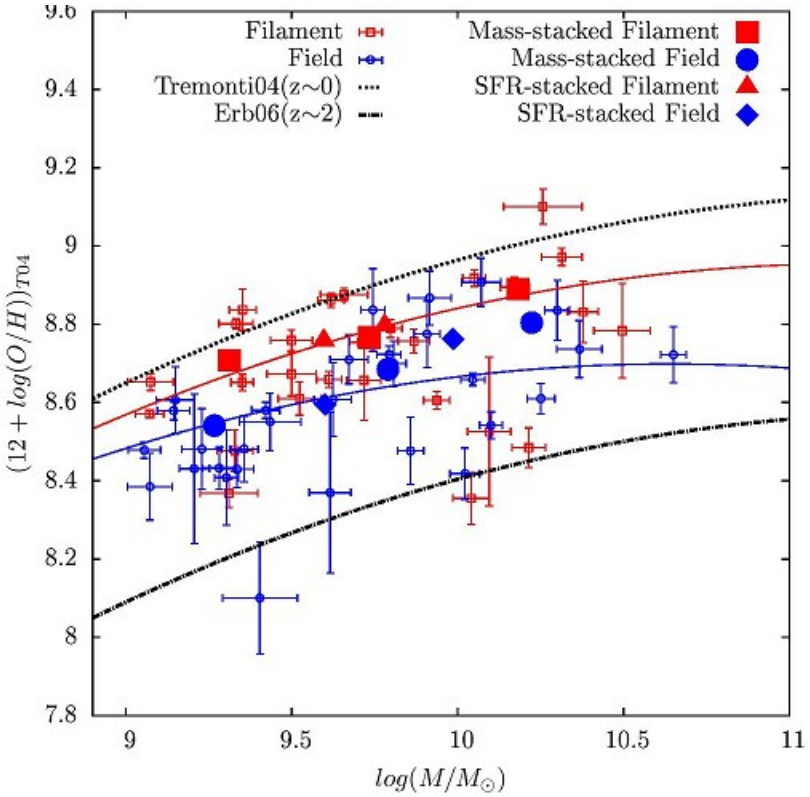


FIG. 9.— Mass-metallicity relation for filament (red empty points) and field (blue empty points) galaxies, along with mass-stacked and SFR-stacked spectra in the filament (red solid points) and the field (blue solid points). Red and blue solid lines represent the fit to the individual galaxies in the filament and the field, respectively. Mass-metallicity relation in the local universe from Tremonti et al. (2004) (dotted line) and that of Erb et al. (2006) at $z \sim 2$ (dashed dotted line) are shown for comparison. The re-

# Astro-ph: 1510.05343

Mon. Not. R. Astron. Soc. **000**, 1–?? (2002) Printed 20 October 2015 (MN LATEX style file v2.2)

# H I-deficient galaxies in intermediate density environments

H. Dénes[1,2⋆], V. A. Kilborn[1], B. S. Koribalski[2], O. I. Wong[3]
[1] *Centre for Astrophysics & Supercomputing, Swinburne University of Technology, PO Box 218, Hawthorn, VIC 3122, Australia*
[2] *Australia Telescope National Facility, CSIRO Astronomy and Space Science, P.O. Box 76, Epping, NSW 1710, Australia*
[3] *International Centre for Radio Astronomy Research, The University of Western Australia M468, 35 Stirling Highway, Crawley, WA 6009, Australia*

# В группах, но с дефицитом HI

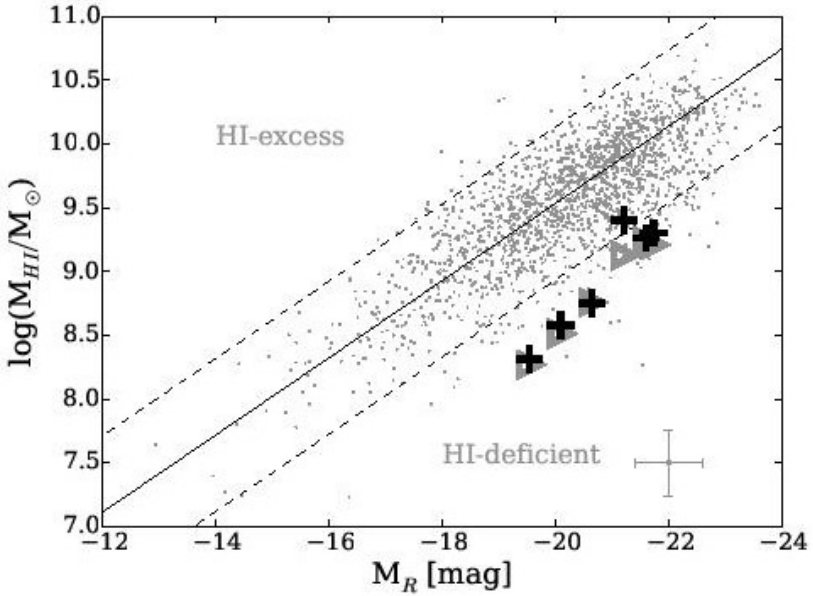


**Figure 1.** $R$-band magnitude versus H I mass for the parent sample. The solid line shows the $R$-band scaling relation from (Dénes et al. 2014) and the dashed line marks $DEF = \pm 0.6$. Grey triangles show the original HICAT H I data for the 6 sample galaxies and black crosses show the re-measured H I mass from the HIPASS data cubes (see Table 3). The error bar displayed in the bottom right indicates the average uncertainties in the data.

# Все HI-диски необычно компактны (+!); а также скособочены (?)

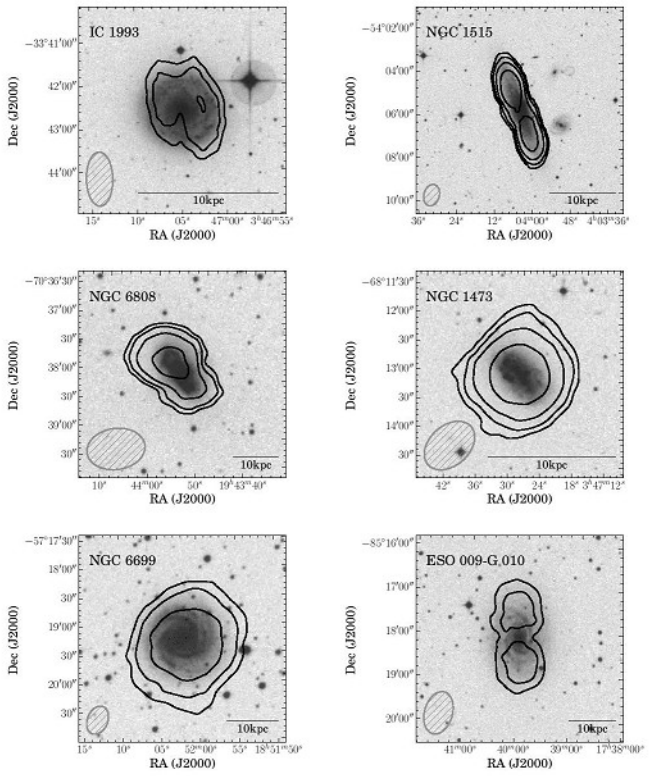


**Figure 2.** H I distribution contours from the combined ATCA data overlaid onto optical B-band images from SuperCOSMOS (UKST).

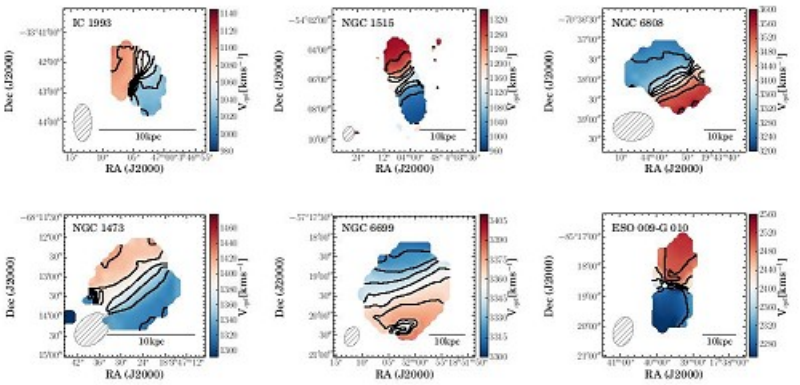


**Figure 3.** H I velocity fields of the sample galaxies. We show the same area and layout as Fig. 2. Dashed lines are velocity contours smaller than the systemic velocity of the galaxies and solid lines are velocity contours larger than the systemic velocity of the galaxies. Velocity contours are spaced 10 km s$^{-1}$ for IC 1993 and NGC 6699, 20 km s$^{-1}$ for NGC 6808 and NGC 1473 and 40 km s$^{-1}$ for NGC 1515 and ESO 009-G 010.

# Выбор сценария

**Table A1.** Summary of the gas removal signatures in each galaxy and the most likely cause of H I-deficiency.

| | IC 1993 | NGC 1515 | NGC 6808 | NGC 1473 | NGC 6699 | ESO 009-G 010 |
|---|---|---|---|---|---|---|
| Small H I disk | ✓ | ✓ | ✓ | ✓ | ✓ | ✓ |
| Lopsided H I disk | ✓ | - | ✓ | - | ✓ | - |
| Asymmetric H I profile | slightly | slightly | ✓ | ✓ | ✓ | slightly |
| Diffuse H I (flux ratios) | 30 % | - | 20% | 25% | 34% | 58% |
| Diffuse H I (H I profile) | ✓ | - | ✓ | - | ✓ | ✓ |
| H I warp | - | ✓ | - | - | - | - |
| Kinematics | slightly pec. | - | - | - | - | slightly pec. |
| Stellar warp | - | - | ✓ | - | - | - |
| Stellar bar | - | - | - | ✓ | - | - |
| Lopsided stellar disk | ✓ | - | ✓ | - | ✓ | ✓ |
| Star formation rate | avg. | avg. | starburst | avg. | increased | avg. |
| Environment | cluster | large group | moderate group | small group | moderate group | triplet |
| Hot IGM | ✓ | ✓ | ✓ | - | - | - |
| likely cause of H I-deficiency: | ram pressure | ram pressure | tidal | tidal? | tidal | tidal? |